

# Boosting Factor-Specific Functional Historical Models for the Detection of Synchronisation in Bioelectrical Signals

David Rügamer

*Department of Statistics, LMU Munich, Munich, Germany.*

Sarah Brockhaus

*Department of Statistics, LMU Munich, Munich, Germany.*

Kornelia Gentsch

*Swiss Center for Affective Sciences, University of Geneva, Geneva, Switzerland.*

Klaus Scherer

*Swiss Center for Affective Sciences, University of Geneva, Geneva, Switzerland.*

Sonja Greven

*Department of Statistics, LMU Munich, Munich, Germany.*

**Summary.** The link between different psychophysiological measures during emotion episodes is not well understood. To analyse the functional relationship between electroencephalography (EEG) and facial electromyography (EMG), we apply historical function-on-function regression models to EEG and EMG data that were simultaneously recorded from 24 participants while they were playing a computerised gambling task. Given the complexity of the data structure for this application, we extend simple functional historical models to models including random historical effects, factor-specific historical effects, and factor-specific random historical effects. Estimation is conducted by a component-wise gradient boosting algorithm, which scales well to large data sets and complex models.

**Keywords:** factor-specific functional historical effect, functional data analysis, function-on-function regression, gradient boosting, signal synchronisation

## 1. Introduction

Bioelectrical signals such as electromyography (EMG), electroencephalography (EEG) or electrocardiogram (ECG) are variations in electrical energy that carry information about living systems (Semmlow and Griffel, 2014). An appropriate analysis of bioelectrical signals, usually obtained in the form of time series data, is a crucial point in many research areas, including (tele-)medicine, automotive technology, and psychology (Kang et al., 2006; Kaniusas, 2012). In the field of cognitive affective neuroscience, a particular interest lies in the link of measured brain activity recorded with the EEG, and peripheral response systems such as the heart rate or facial muscle activity. In this context, our motivating study (Gentsch et al., 2014) investigated the coherence between emotion components. In componential emotion theory, an emotional episode is thought to be an emergence of coherent or temporally correlated changes in emotion components, such as appraisals or facial expressions. This is referred to as synchronisation (Grandjean and Scherer, 2009).

*The emotion components data.* In the study of Gentsch et al., brain activity (EEG) as well as facial muscle activity (EMG) was simultaneously recorded. The data set at hand consists of time series of 384 equidistant observed time points for both EEG and EMG signals, eight different study settings (conditions in a computerised gambling game) and 24 participants. The traditional approach of analysing EEG and EMG data is to calculate the average signal for each participant across all trials of one study setting. For EEG data, this is referred to as event-related potential analysis (see, e.g., Pfurtscheller and da Silva, 1999). Such an aggregation yields a reduced data set of  $N = 8 \cdot 24 \cdot 384 = 73,728$  observed data points. At each of the  $N$  time points, measurements are available for three EMG and 64 EEG electrodes. Figure 1 depicts one EEG and EMG signal for one participant and all eight study settings with a common starting point of  $200ms$  after stimulus onset.

Efferent signals from the brain (signals originating from the brain) innervate or activate facial muscles (see, e.g., Rinn, 1984). Therefore, it should be possible to trace back facial muscle activity recorded with facial EMG to brain activity captured with EEG. As certain cognitive processes can be related to different brain areas and facial regions, our particular interest lies in investigating the link between a selected EEG electrode signal and a specific EMG signal. We expect any association between these two signals to (a) be time-varying, (b) exhibit a temporal lag that is a priori unknown (even though a minimum lag can be inferred from the literature), (c) be specific to a study setting and / or (d) be only present during certain time intervals.

*Existing methods for detecting synchronisation.* Previous approaches to detect synchrony in brain activity and autonomic physiology data have mostly focused on coherence or cross-correlation. Examinations of EEG and EMG synchronisation can, inter alia, be found in Hollenstein

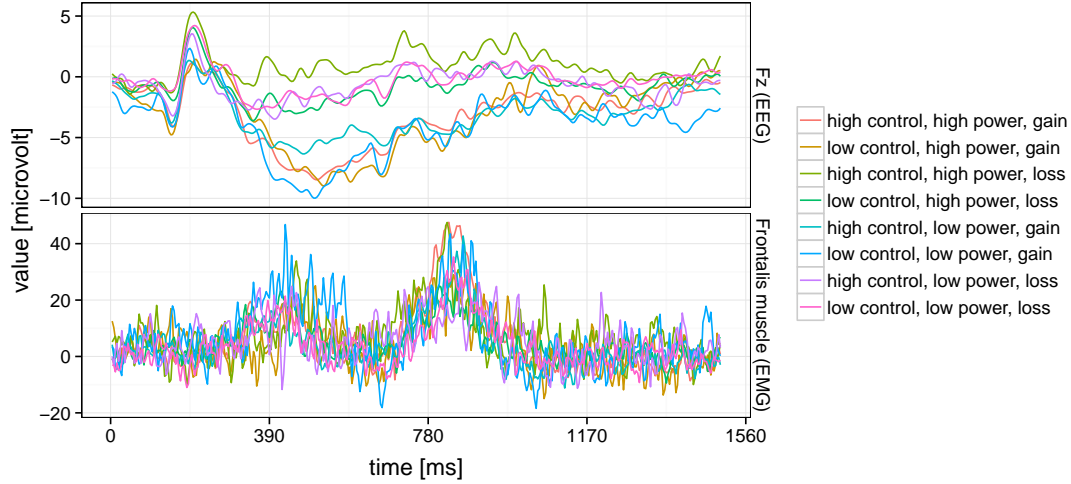


Fig. 1: Example for one EEG signal (Fz electrode) and one EMG signal (frontalis muscle for raising eyebrows) of one participant, averaged over all trials for each of the eight possible game conditions (line colours)

and Crowell (2014); Mima and Hallett (1999); Brown (2000); Mima et al. (2000a,b); Grosse et al. (2002); Quiroga et al. (2002); Bortel and Sovka (2006); Hashimoto et al. (2010). While coherence is a function of the frequency measuring the explained variance of one time series by another time series in the frequency-domain, cross-correlation is a function of time, yielding the correlation of two time series for a given lag (see, e.g., Pawitan, 2005). With the aim to relate different time points of two signals to each other, we focus on methods in the time-domain. Established methods are, however, concerned with the estimation of the association between two observed time series rather than the analysis of a large number of time series observations given in pairs of two signals. This applies for (cross-)correlation, which additionally does not provide the possibility to take covariates into account, as well as for other methods such as the *generalised synchronisation* approach based on the state-space representation (Diab et al., 2013) or autoregressive times series approaches (see e.g. Ozaki, 2012). Furthermore, most of these approaches require the definition of a specific or a maximum time lag.

*Function-on-function regression.* As both the EEG and the EMG signal can be understood as noisy observations of functional variables, function-on-function regression approaches offer another possibility to describe and infer the relationship of such time series (see Morris, 2015, for a recent review). Function-on-function regression models adapt the principle of standard regression by allowing for a functional response as well as functional covariates. The so called historical model (Malfait and Ramsay, 2003; Harezlak et al., 2007) is one possibility to explain a functional response  $Y(t), t \in \mathcal{T} = [T_1, T_2]$  with  $T_1, T_2 \in \mathbb{R}$ , using a linear effect of the complete

history of a functional covariate  $X(s), s \in \mathcal{T}$ :

$$\mathbb{E}(Y(t)|X = x) = \int_{T_1}^t x(s)\beta(s, t)ds. \quad (1)$$

In contrast to the existing approaches discussed above, historical models allow us to relate a given time point of one time series to more than one time point in  $[T_1, t]$  of another time series.

Early core work on functional historical models is limited to historical models with only one functional covariate. A multitude of application possibilities are conceivable and historical models have been used in different research areas including health and biological science (Malfait and Ramsay, 2003; Harezlak et al., 2007; Gervini, 2015; Brockhaus et al., 2016b). Brockhaus et al. (2016b) extended the framework of a simple historical model as in (1) to functional regression models with a high number of functional historical effects and potentially further covariate effects by utilizing gradient boosting for estimation.

Alternative estimation procedures for flexible function-on-function regression models including historical effects are based on a mixed model representation (cf. Scheipl et al., 2015) or component-wise gradient boosting (cf. Brockhaus et al., 2015, 2016b). These are implemented in the `pffr`-function of the R package `refund` (Huang et al., 2015) and in the R package `FDboost` (Brockhaus and Rügamer, 2016), respectively.

*Proposed approach.* In order to reflect the study design in this application, we extend functional historical models to historical effects that vary over one or two (penalised) categorical covariates to allow for subject-, setting- and subject-by-setting-specific effects. We provide mathematical concepts for the construction of design matrices, penalty matrices as well as suitable identifiability constraints. We integrate these concepts into the framework of Brockhaus et al. (2015, 2016b) and implement them for estimation via component-wise gradient boosting. We also speed up the estimation by making use of our particular model structure. By carrying out estimation with component-wise gradient boosting as in Brockhaus et al. (2015), our approach has several advantages. In particular, it can fit multiple factor-, subject- as well as subject-by-factor-specific functional effects, which is not possible in alternative approaches for function-on-function regression such as implemented in the `pffr`-function in the R package `refund` (Huang et al., 2015). Furthermore, the algorithm allows for different loss functions and thus covers models beyond mean regression (Kneib, 2013), e.g., median, robust or quantile regression. It can deal with high-dimensional data sets that often go hand in hand with multi-sensor bioelectrical signal data collections, as well as settings with more covariates than observations. Our approach is able to find multi-modal effect surfaces and band effects, thereby covering special cases of time series approaches. In addition, we derive options to reduce computation time as well as memory

storage considerably and address the question of uncertainty in complex boosted models.

The remainder of this paper describes the proposed model and method in section 2, presents the gradient boosting algorithm in section 3 and covers a simulation study in section 4. We apply boosted historical models to the emotion components data in section 5 and conclude with a discussion in section 6. Our proposed methods are implemented in the R package `FDboost`, an extension of the model based boosting package `mboost` (Hothorn et al., 2016). The R code for our simulation as well as code and data for our application is provided in an online repository (<https://github.com/davidruegamer/BoostingSignalSynchro>).

## 2. Functional response models and historical effects

After outlining the functional historical model in 2.1, we extend the model of Brockhaus et al. (2016b) to models with functional historical terms interacting with categorical covariates and to random functional historical effects in subsection 2.2.

### 2.1. Functional historical models

We focus on additive functional regression models of the form (Brockhaus et al., 2015, 2016b)

$$\xi(Y(t)|\mathbf{X} = \mathbf{x}) = h(\mathbf{x})(t) = \sum_{j=1}^J h_j(\mathbf{x})(t), \quad (2)$$

where  $\xi$  is a transformation function for the conditional distribution of the functional response  $Y(t), t \in \mathcal{T}$ . In our application  $\xi$  is equal to the conditional expectation  $\mathbb{E}$ , although it could also be e.g. the (pointwise) median or a quantile. The covariate set  $\mathbf{x}$  comprises functional observations  $x_1(\cdot), \dots, x_{p_x}(\cdot)$  and scalar covariates  $z_1, \dots, z_{p_z}$  with  $p := p_x + p_z$ .  $h_j(\mathbf{x})(t)$  are partial effects, which can depend on scalar as well as on functional covariates. In particular, this general model class includes models with one or more historical effects

$$h_j(\mathbf{x})(t) = \int_{l(t)}^{u(t)} x_{k_j}(s) \beta_j(s, t) ds, \quad (3)$$

$k_j \in \{1, \dots, p_x\}$ , which can have general integration limits  $l(t)$  and  $u(t)$ , e.g., defined by  $l(t) = T_1$  and  $u(t) = t$ ,  $l(t) = t - \delta$  and  $u(t) = t$  or partial histories  $l(t) = t - \delta_l$  and  $u(t) = t - \delta_u$ ,  $t > \delta_l > \delta_u > 0$  as in Harezlak et al. (2007). Functional historical effects are particularly suited to settings where both response  $Y(t)$  and covariates  $X_{k_j}(s)$  are observed over the same time interval,  $s, t \in \mathcal{T}$ .

In practice,  $x_{k_j}(\cdot)$  is observed on a grid  $s_1, \dots, s_R$  and the integral as well as the smooth

coefficient surface  $\beta_j(s, t)$  in (3) must be approximated. We use numerical integration and a tensor product spline basis expansion, respectively. For  $k = 1, \dots, K_x, l = 1, \dots, K_t$  define the basis functions  $\Phi_{j,k}^s(s)$  and  $\Phi_{j,l}^t(t)$  for the  $s$ - and the  $t$ -direction of the coefficient surface  $\beta_j(s, t)$ , respectively. Let  $\theta_{j,k,l}$  be the corresponding basis coefficients and  $\Delta(s_r)$  numerical integration weights for the observed time points  $s_r$ . Then, the historical effect can be represented by (Scheipl et al., 2015; Brockhaus et al., 2016b)

$$\int_{l(t)}^{u(t)} x_{k_j}(s) \beta_j(s, t) ds \approx \mathbf{B}_j(x_{k_j}, t) \boldsymbol{\theta}_j \quad (4)$$

with  $\boldsymbol{\theta}_j = (\theta_{j,1,1}, \dots, \theta_{j,K_x,K_t})^\top$ ,  $\mathbf{B}_j(x_{k_j}, t) = \mathbf{B}_j^x(x_{k_j}, t) \otimes \mathbf{B}_j^t(t)$  using the Kronecker-product  $\otimes$  and by defining

$$\mathbf{B}_j^x(x_{k_j}, t) = \left[ \sum_{r=1}^R \Delta(s_r) x_{k_j}(s_r, t) \Phi_{j,1}^s(s_r) \cdots \sum_{r=1}^R \Delta(s_r) x_{k_j}(s_r, t) \Phi_{j,K_x}^s(s_r) \right]$$

as well as  $\mathbf{B}_j^t(t) = [\Phi_{j,1}^t(t) \cdots \Phi_{j,K_t}^t(t)]$ . Let  $I(\cdot)$  be the indicator function. Following Scheipl et al. (2015), for  $n$  observed curves  $x_{k_j,1}(\cdot), \dots, x_{k_j,n}(\cdot)$  at grid points  $s_r$ ,  $x_{k_j}(s_r, t) = x_{k_j}(s_r) \cdot I\{l(t) \leq s_r \leq u(t)\}$  and response observations  $y_i(t_{i,d})$  at potentially curve specific time points  $t_{i,d} \in \mathcal{T}, i = 1, \dots, n, d = 1, \dots, D_i, N = \sum_{i=1}^n D_i$ , the design matrix of a historical effect can be summarised by

$$\mathcal{B}_j := \mathbf{B}_j^x \odot \mathbf{B}_j^t = (\mathbf{B}_j^x \otimes \mathbf{1}_{K_t}^\top) * (\mathbf{1}_{K_x}^\top \otimes \mathbf{B}_j^t), \quad (5)$$

where  $\mathbf{B}_j^x \in \mathbb{R}^{N \times K_x}$  with rows  $\mathbf{B}_j^x(x_{k_j,i}, t_{i,d})$ ,  $\mathbf{B}_j^t \in \mathbb{R}^{N \times K_t}$  with rows  $\mathbf{B}_j^t(t_{i,d})$ ,  $\odot$  is the row-wise tensor product,  $*$  the Hadamard product (element-wise matrix multiplication) and  $\mathbf{1}_a^\top$  a row-vector of length  $a$ . In the supplemental material, we provide a simple example of how to interpret estimated coefficient surfaces of historical effects, as we believe that this is an important part in using historical models.

Regularisation of the coefficient vector  $\boldsymbol{\theta}_j$  in (4) is achieved by an anisotropic penalty. Using the marginal penalties  $\mathbf{P}_j^x \in \mathbb{R}^{K_x \times K_x}$  and  $\mathbf{P}_j^t \in \mathbb{R}^{K_t \times K_t}$  of the historical effect basis in  $s$ - and  $t$ -direction, respectively, a quadratic penalty term can be constructed as

$$\boldsymbol{\theta}_j^\top \mathcal{P}_j \boldsymbol{\theta}_j = \boldsymbol{\theta}_j^\top [\lambda_j^x (\mathbf{P}_j^x \otimes \mathbf{I}_{K_t}) + \lambda_j^t (\mathbf{I}_{K_x} \otimes \mathbf{P}_j^t)] \boldsymbol{\theta}_j = \boldsymbol{\theta}_j^\top [\lambda_j^x \mathbf{P}_j^x \oplus \lambda_j^t \mathbf{P}_j^t] \boldsymbol{\theta}_j, \quad (6)$$

where  $\lambda_j^x, \lambda_j^t \geq 0$  are smoothing parameters and  $\oplus$  is the Kronecker-sum (Wood, 2006; Scheipl et al., 2015). More details on the penalisation and potential extensions can be found in the next subsection. Similarly, penalised basis expansions as in (4), (5), and (6) can also be constructed for a multitude of other effects of scalar and / or functional covariates, including all effects of scalar covariates in our proposed model for the emotion components data (Scheipl et al., 2015;

Brockhaus et al., 2015).

In addition to ordinary historical effects, this approach can incorporate a time-varying intercept  $h_j(\mathbf{x})(t) = \alpha(t)$  as well as time-varying categorical or random effects

$$h_j(\mathbf{x})(t) = \gamma_{j,e}(t) \cdot I(z_{q_j} = e), \quad (7)$$

where  $q_j \in \{1, \dots, p_z\}$ ,  $z_{q_j}$  is a categorical covariate with levels  $e \in \{1, \dots, \eta\}$  and  $\gamma_{j,e}(t)$  the corresponding time-varying coefficient. The smoothness of the coefficient functions  $\alpha(t)$  and  $\gamma_{j,e}(t)$  is obtained with a spline basis representation as in (4) and a Kronecker sum penalty as in (6) with  $\mathbf{P}_j^x$  set to zero for categorical effects and  $\mathbf{P}_j^x = \mathbf{I}_{K_z}$  for (independent) functional random effects (see Brockhaus et al., 2015, for more details). In particular, for functional random effects, the quadratic penalty in (6) is equivalent to a normal distribution assumption on  $\theta_j$  with zero mean and covariance proportional to the generalised inverse of  $\mathcal{P}_j$  (Brumback et al., 1999), inducing a Gaussian process assumption for the functional random effects. Furthermore, we consider interaction effects of  $z_{q_j}$  and a second categorical covariate  $z_{q'_j}$  with levels  $f = 1, \dots, \varphi$  of the form

$$h_j(\mathbf{x})(t) = \rho_{j,e,f}(t) \cdot I(z_{q_j} = e) \cdot I(z_{q'_j} = f). \quad (8)$$

Identifiability constraints for time-varying categorical effects such as (7) and (8) are discussed in the following subsection.

## 2.2. Factor-specific historical effects

In light of our application, we newly introduce factor-specific historical effects for functional regression models. Factor-specific historical effects can be useful when historical effects are assumed to vary, e.g., between different study settings or subjects. First, consider a categorical covariate  $z_{q_j}$  with levels  $e = 1, 2, \dots, \eta$  and a functional covariate  $x_{k_j}(s)$ , which is modeled via a historical effect. A simple additive model of the form (2) would then include a main historical effect (3) and a factor-specific historical effect

$$h_j(\mathbf{x})(t) = I(z_{q_j} = e) \cdot \int_{l(t)}^{u(t)} x_{k_j}(s) \beta_{j,e}(s, t) ds. \quad (9)$$

Given a total of  $N$  observations and the covariate vector  $\mathbf{z}_{q_j} = [(z_{q_j,1} \otimes \mathbf{1}_{D_1})^\top, \dots, (z_{q_j,n} \otimes \mathbf{1}_{D_n})^\top]^\top$  the factor-specific historical effect is constructed similarly to (5). The design matrix is extended to

$$\mathbf{B}_j = \mathbf{B}_j^z(\mathbf{z}_{q_j}) \odot \mathbf{B}_j^x \odot \mathbf{B}_j^t = \tilde{\mathbf{B}}_j^x \odot \mathbf{B}_j^t, \quad (10)$$

where  $\mathbf{B}_j^z(\mathbf{z}_{q_j})$  is a design matrix for the factor variable depending on the constraints on  $\beta_{j,e}(s, t)$  (see below) and  $\tilde{\mathbf{B}}_j^x = \mathbf{B}_j^z(\mathbf{z}_{q_j}) \odot \mathbf{B}_j^x$ . An important special case is given for the unconstrained estimation of  $\beta_{j,e}$  when the observations are sorted by the factor levels  $e = 1, \dots, \eta$ . This yields a block-diagonal incidence matrix for  $\mathbf{B}_j^z(\mathbf{z}_{q_j}) = \text{diag}(\mathbf{1}_{\kappa_1}, \mathbf{1}_{\kappa_2}, \dots, \mathbf{1}_{\kappa_\eta}) \in \mathbb{R}^{N \times \eta}$  and a  $N \times \eta K_x$  block-diagonal matrix for  $\tilde{\mathbf{B}}_j^x = \text{diag}(\mathbf{B}_{j,1}^x, \dots, \mathbf{B}_{j,\eta}^x)$ . Here,  $\mathbf{B}_{j,e}^x \in \mathbb{R}^{\kappa_e \times K_x}$  contains the rows  $\sum_{k=1}^{e-1} \kappa_k + 1, \dots, \sum_{k=1}^e \kappa_k$  of  $\mathbf{B}_j^x$  corresponding to all rows with factor level  $e$  and  $\kappa_e$  being the total number of observation points for factor level  $e$ . This special structure can be exploited for a more efficient computational implementation (see section 3.2 for more details).

When the historical effect of  $x_{k_j}$  is not only factor- or subject-specific, but varies for a categorical covariate  $z_{q_j}$  with levels  $e = 1, 2, \dots, \eta$  as well as for subjects  $z_{q'_j}$  with levels  $f = 1, 2, \dots, \varphi$ , we let

$$h_j(\mathbf{x})(t) = I(z_{q_j} = e) \cdot I(z_{q'_j} = f) \cdot \int_{l(t)}^{u(t)} x_{k_j}(s) \beta_{j,e,f}(s, t) ds. \quad (11)$$

The design matrix for the random factor-specific historical effect or *doubly-varying historical effect* (11) is then defined by extending  $\mathbf{B}_j^z(\mathbf{z}_{q_j})$  in (10) to

$$\mathbf{B}_j^z(\mathbf{z}_{q_j}, \mathbf{z}_{q'_j}) = \mathbf{B}_j^z(\mathbf{z}_{q_j}) \odot \mathbf{B}_j^z(\mathbf{z}_{q'_j}).$$

For these factor-specific historical effects (9) and (11), we have to carefully consider their identifiability and regularisation.

*Identifiability constraints.* In order to ensure that the main historical effect is separable from the factor-specific historical effects and vice versa, we impose the following constraint when both are included in the model:

$$\sum_{e=1}^{\eta} \psi_e \cdot \beta_{j,e}(s, t) = 0 \quad \forall t \in \mathcal{T}, s \in [l(t), u(t)], \quad (12)$$

where  $\psi_e$  are weights for each level  $e = 1, \dots, \eta$  of the factor variable. Specifically, for observed curves  $i = 1, \dots, n$ , we use  $\psi_e = \sum_{i=1}^n I(z_{q_j, i} = e)$ , which coincides with equal weighting in the case of balanced factor levels. This also allows  $\beta_j(s, t)$  in (9) to be interpretable as average historical effect over the  $\eta$  subgroups. (12) ensures identifiability because the factor-specific historical effects are centred around the surface of the main effect for models including both (3) and (9).

For the doubly-varying historical effects to be defined as deviations from both factor-specific



historical effects, we impose the constraints

$$\sum_{e=1}^{\eta} \psi_{e,f} \cdot \beta_{j,e,f}(s,t) = 0 \quad \forall t \in \mathcal{T}, s \in [l(t), u(t)], f \in \{1, \dots, \varphi\} \quad \text{and} \quad (13)$$

$$\sum_{f=1}^{\varphi} \psi_{e,f} \cdot \beta_{j,e,f}(s,t) = 0 \quad \forall t \in \mathcal{T}, s \in [l(t), u(t)], e \in \{1, \dots, \eta\}, \quad (14)$$

for which we use the weights  $\psi_{e,f} = \sum_{i=1}^n I(z_{q_j,i} = e, z_{q'_j,i} = f)$ .

To ensure identifiability and interpretability of the whole model, further constraints must be placed on effects other than the historical effects, i.e., when including time-varying effects in the model. As in [Scheipl et al. \(2015\)](#) and [Brockhaus et al. \(2015\)](#), all time-varying effects in our models are specified as deviations from the smooth intercept  $\alpha(t)$ . This ensures the identifiability of each effect and allows for a meaningful interpretation (as deviation from the sample mean  $\alpha(t)$ ). Consider the factor variable  $z_{q_j}$  and an effect as in (7). We then impose  $\sum_{e=1}^{\eta} \psi_e \cdot \gamma_{j,e}(t) = 0 \forall t \in \mathcal{T}$ . A similar constraint is enforced for interaction effects (8) with coefficients  $\rho_{j,e,f}(t)$ :  $\sum_{e=1}^{\eta} \psi_{e,f} \cdot \rho_{j,e,f}(t) = 0 \forall t \in \mathcal{T}, f \in \{1, \dots, \varphi\}$  and  $\sum_{f=1}^{\varphi} \psi_{e,f} \cdot \rho_{j,e,f}(t) = 0 \forall t \in \mathcal{T}, e \in \{1, \dots, \eta\}$ , i.e., each interaction effect has to be centred around its corresponding main effects. For details on the implementation, see section B in the supplementary material.

*Parameterisation.* The separation of the factor-specific historical effect and the corresponding main historical effect together with constraint (12) is particularly useful in the light of model selection. However, an alternative model formulation that does not separate main and factor-specific historical effects may sometimes be beneficial for the interpretation of estimated effects and the simplicity of the model definition. A historical model with a main and factor-specific historical effects can be rewritten as  $\int_{l(t)}^{u(t)} x_{k_j}(s) \left( \beta_j(s,t) + I(z_{q_j} = e) \cdot \beta_{j,e}(s,t) \right) ds$ , combining main and factor-specific historical effects by estimating the sum  $\tilde{\beta}_{j,e}(s,t) := (\beta_j(s,t) + I(z_{q_j} = e) \cdot \beta_{j,e}(s,t))$  and thereby making constraint (12) obsolete.

*Regularisation.* For the regularisation of a factor-specific historical effect, the penalty depends on whether we want to regularise over the factor levels, e.g., for “*random historical effects*”, or not, e.g., for study settings. In general, the quadratic penalty matrix in (6) is extended to an anisotropic penalty

$$\mathcal{P}_j = \left( \lambda_j^z \mathbf{P}_j^z \oplus \left[ \lambda_j^x \mathbf{P}_j^x \oplus \lambda_j^t \mathbf{P}_j^t \right] \right), \quad (15)$$

where  $\mathbf{P}_j^z$  is the  $K_z \times K_z$  marginal penalty matrix over the factor levels and  $\lambda_j^x, \lambda_j^t, \lambda_j^z$  are the smoothing parameters controlling the regularisation of the historical effect part in  $s$ - as well as  $t$ -direction and of the factor variable part, respectively. Usually,  $K_z$  is the number of factor levels (minus one, depending on the constraint on the effect) and  $\mathbf{P}_j^z$  is a simple Ridge penalty  $\mathbf{P}_j^z = \mathbf{I}_{K_z}$ . Whereas the factor-specific historical effect is therefore shrunk towards the main

historical effect in a model with both, main and factor-specific historical effect, the penalty in the alternative parametrisation without constraint on the factor-specific historical effect enforces shrinkage of  $\beta_{j,e}$  towards zero. In practice, the  $s$ - and  $t$ -directions of the historical effect are typically measured on the same scale (i.e., time), thus we introduce an isotropic penalty for the historical effect part by defining  $\lambda_j^t \equiv \lambda_j^x =: \lambda_j^h$  and  $\mathbf{P}_j^x \oplus \mathbf{P}_j^t =: \mathcal{P}_j^h$ . For the doubly-varying historical effect (11), the term  $\lambda_j^z \mathbf{P}_j^z$  in (15) is replaced by  $[\lambda_j^z \mathbf{P}_j^z \oplus \lambda_j^{z'} \mathbf{P}_j^{z'}]$ . If one or both factors are not penalised, the corresponding penalty matrices are set to zero.

### 3. Estimation: Component-wise gradient boosting

The estimation via component-wise gradient boosting (Bühlmann and Hothorn, 2007; Brockhaus et al., 2015) has several advantages. The main advantage of using component-wise boosting over conventional estimation procedures lies in the nature of component-wise fitting, as the feasibility of component-wise fitting procedures only depends on the most complex individual component. Adding partial effects step-by-step, boosting provides implicit variable selection and allows for model estimation in settings with  $J > n$  or  $p > n$ .

#### 3.1. Component-wise gradient boosting

The component-wise gradient boosting algorithm for a function-on-function regression model was introduced by Brockhaus et al. (2015), and is based on the functional gradient descent (FGD) algorithm (cf. Bühlmann and Hothorn, 2007; Hothorn et al., 2016).

*Loss function and empirical risk.* In general, the component-wise FGD algorithm aims to minimize the expected loss  $\mathbb{E}_{(Y, \mathbf{X})}(\rho((Y, \mathbf{X}), h))$  for response  $Y$  and covariates  $\mathbf{X}$  with respect to the additive predictor  $h$  for a suitable loss function  $\rho$ . The loss is determined by the underlying regression problem, e.g., the  $L^2$ -loss for mean regression. In order to adapt the principle of FGD to functional observations, the loss function  $\ell$  for a whole trajectory is defined as  $\ell((Y, \mathbf{X}), h) = \int_{\mathcal{T}} \rho((Y, \mathbf{X}), h)(t) dt$ , i.e., the integrated pointwise loss  $\rho$  over the domain  $\mathcal{T}$ . For potentially functional observations  $(y_i, \mathbf{x}_i), i = 1, \dots, n$ , the objective function, the risk, is then given by  $\mathbb{E}_{(Y, \mathbf{X})}(\ell((Y, \mathbf{X}), h))$  and the FGD algorithm for functional regression models aims at minimizing the empirical risk

$$n^{-1} \sum_{i=1}^n \sum_{d=1}^{D_i} w_i \Upsilon(t_{i,d}) \rho((y_i, \mathbf{x}_i), h)(t_{i,d}),$$

where sampling weights  $w_i$  are used to select or deselect all observations of one functional trajectory in resampling approaches and  $\Upsilon(t)$  are weights of a numerical integration scheme used to approximate the integrated loss  $\ell$  (Brockhaus et al., 2016b).

*Routine and baselearners.* In each step, the FGD algorithm evaluates a set of *baselearners* (in this case corresponding to penalised regression for the partial effects  $h_j$ ), chooses the baselearner that best fits the negative gradient at the current estimate  $-\frac{\partial}{\partial h}\mathbb{E}_{(Y, \mathbf{X})}(\ell((Y, \mathbf{X}), h))$  and updates the fit in light of this choice. As in representation (4), we assume that every baselearner can be represented as a linear effect in  $\boldsymbol{\theta}_j \in \mathbb{R}^{K_j}$ , i.e.  $h_j(\mathbf{x})(t) = \mathbf{B}_j(\mathbf{x}_{k_j}, t)\boldsymbol{\theta}_j$ , with suitable penalty, e.g., (6) or (15).

*Algorithm.* The full algorithm is given by the following five steps:

*Step 1:* Set  $m = 0$ ; Initialise the estimates, e.g.  $\hat{\boldsymbol{\theta}}_j^{[m]} \equiv \mathbf{0}$  for each baselearner  $j \in \{1, \dots, J\}$ , and define  $\hat{h}^{[m]}(\mathbf{x})(t) = \sum_{j=1}^J \mathbf{B}_j(\mathbf{x}, t)\hat{\boldsymbol{\theta}}_j^{[m]}$ ; choose a step-length  $\nu \in (0, 1]$  and a maximal stopping iteration  $m_{\text{stop}}$ .

*Step 2:* Compute the negative gradient  $-\frac{\partial}{\partial h}\rho((y, \mathbf{x}), h)$  and define the so called *pseudo residuals*

$$u_i(t_{i,d}) := -\frac{\partial}{\partial h}\rho((y_i, \mathbf{x}_i), h)(t_{i,d}) \Big|_{h=\hat{h}^{[m]}}.$$

*Step 3:* Fit the baselearners  $j = 1, \dots, J$  to the pseudo residuals

$$\hat{\boldsymbol{\theta}}_j = \underset{\boldsymbol{\vartheta} \in \mathbb{R}^{K_j}}{\operatorname{argmin}} \sum_{i=1}^n \sum_{d=1}^{D_i} w_i \Upsilon(t_{i,d}) \left\{ u_i(t_{i,d}) - \mathbf{B}_j(\mathbf{x}_{k_j,i}, t_{i,d})\boldsymbol{\vartheta} \right\}^2 + \boldsymbol{\vartheta}^\top \mathcal{P}_j \boldsymbol{\vartheta}$$

and find the best-fitting  $j^*$ th baselearner such that

$$j^* = \underset{j=1, \dots, J}{\operatorname{argmin}} \sum_{i=1}^n \sum_{d=1}^{D_i} w_i \Upsilon(t_{i,d}) \left\{ u_i(t_{i,d}) - \mathbf{B}_j(\mathbf{x}_{k_j,i}, t_{i,d})\hat{\boldsymbol{\theta}}_j \right\}^2.$$

*Step 4:* Set  $\hat{\boldsymbol{\theta}}_{j^*}^{[m+1]} = \hat{\boldsymbol{\theta}}_{j^*}^{[m]} + \nu \hat{\boldsymbol{\theta}}_{j^*}$ ,  $\hat{\boldsymbol{\theta}}_j^{[m+1]} = \hat{\boldsymbol{\theta}}_j^{[m]} \forall j \neq j^*$  and update  $\hat{h}^{[m]}$  accordingly.

*Step 5:* Set  $m = m + 1$ ; as long as  $m \leq m_{\text{stop}}$ , repeat steps 2 — 5.

The final model with corresponding parameters  $\hat{\boldsymbol{\theta}}_j^{m^*}$ ,  $j = 1, \dots, J$ ,  $m^* \in \{1, \dots, m_{\text{stop}}\}$  is chosen from the set of  $m_{\text{stop}}$  estimated models via cross-validation or other resampling methods on the level of curves (Brockhaus et al., 2015) in order to prevent over-fitting. This so called early stopping of the boosting procedure introduces regularisation on coefficient estimates (Zhang and Yu, 2005).

### 3.2. Unbiased baselearner selection and smoothing parameter computation

It is important to set equal degrees of freedom  $df_j$  for every baselearner  $j$  for a fair selection of baselearners (Hofner et al., 2011). A regularisation over factor levels for categorical covariates with a moderate or large number of factor levels is thus often necessary in practice as  $df_j$  would

otherwise become very large. The smoothing parameters  $\lambda_j$ , which have a one-to-one correspondence with  $df_j$ , must therefore be computed and fixed appropriately beforehand for  $j = 1, \dots, J$ . Model complexity and smoothness is then controlled for fixed  $\nu$  by the stopping iteration, which is chosen by resampling.

The `FDboost` package, based on the `mboost` package, uses the Demmler-Reinsch orthogonalization (DRO, see, e.g., [Ruppert et al., 2003](#)), which avoids repeated matrix inversions to efficiently find a suitable  $\lambda_j$ . Nonetheless, computing the DRO may be very expensive, particularly for factor- and subject-specific historical effects, due to a singular value decomposition (SVD), and can take up to 99% of total computing time. To tackle this problem, on the one hand, we recommend reducing the number of knots for (doubly-)varying historical effects to a small number (e.g., four), if this is not expected to lead to unwanted oversmoothing. On the other hand, we exploit the model structure for factor-specific historical effects and derive a presentation that allows for a blockwise SVD with computation time on the order of an ordinary historical effect. This reduces overall computation time dramatically (see section C in the supplementary material for more details). For the application in section 5, for example, the most complex model with partially aggregated data could be fitted in under 16 minutes with less than 45 gigabyte RAM, whereas the brute-force method (fitting the model with ten knots without exploitation of the model structure) failed, exceeding the memory limit of 1 terabyte RAM after running for more than 10 days. Although the first approach can be a good (approximate) ad-hoc solution, the second approach is exact and thus generally recommended if feasible.

### 3.3. *Quantification of uncertainty*

Due to the large fluctuation in bioelectrical signals, a very important aspect in the analysis of such signals is the assessment and quantification of uncertainty. For the detection of synchronisation with a large number of potentially relevant time intervals of both signals, “significant” effects for specific time point combinations are of particular interest. Apart from rank based p-values provided in the context of Likelihood-based boosting ([Binder et al., 2009](#)) using permutations of the response, no general inferential framework in the classical statistical sense exists for boosting methods. An alternative approach is stability selection ([Meinshausen and Bühlmann, 2010](#)), which evaluates the importance of explanatory variables by looking at the stability of term selection under subsampling and has already been adapted for functional regression boosting (see e.g., [Brockhaus et al., 2015](#)). In the emotion components application, however, the applied research question defines the chosen covariates and the statistical analysis needs to address the uncertainty of estimated coefficient surfaces. We therefore use a non-parametric curve-level bootstrap to assess the variability of estimated effects. Due to the shrinkage effect of boosting,

the corresponding bootstrap intervals are useful for variability quantification of the regularised coefficients, but are on average not centred at the true coefficient surface, unlike unbiased estimators. In consequence, the distribution of bootstrap estimates does not provide valid confidence intervals. In the following section, we investigate whether despite the shrinkage effect, variability bands can be used at least to assess point-wise difference from zero. As simulation results suggest, these variability bands find most of the truly non-zero surface regions in all of our simulation settings.

#### 4. Simulations

We provide results for the estimation performance of simple historical effects (subsection 4.1), factor-specific historical effects (subsection 4.2) and for the uncertainty quantification via bootstrap (subsection 4.3). In section 4.4, we briefly address results on different parametrisations and boosting step-lengths.

Similar to our application, we use historical effects with integration limits  $l(t) = T_1 = 0$  and  $u(t) = t - \delta$  with  $\delta = 0.025$ . We compare the estimated surface with the underlying true function and, wherever possible, with an estimate using a functional additive mixed model as implemented in the `pffr`-function in R package `refund` (Scheipl et al., 2015). Apart from visual comparisons, we estimate the relative integrated mean squared error (*reliMSE*)  $\iint (\hat{\beta}(s, t) - \beta(s, t))^2 ds dt \cdot (\iint \beta(s, t)^2 ds dt)^{-1}$  by its discrete approximation in order to compare the estimates of our method, referred to as `FDboost`.

Simulation settings were generally based on  $n \in \{80, 160, 320, 640\}$  number of observed curves with  $D_i \equiv D \in \{20, 40, 60\}$  observed grid points per trajectory, a *signal-to-noise ratio*  $\text{SNR} \in \{0.1, 1, 10\}$ . For the following subsections the combinations were customised or restricted accordingly, in particular for simulations with very time-consuming bootstrap calculations. Whereas the number of curves in our application  $n = 184$  is within the range of simulated settings, we use fewer observations per trajectory in our simulations than available in our application ( $D = 384$ ) in order to reduce computational time. Increasing sampling density  $D$  from 60 to 180 or 380 in additional simulations with  $\text{SNR} \in \{0.01, 0.1, 1\}$  and  $n = 160$  almost always results in an improvement of estimation performance. The average estimated SNR in our application is 0.42, which, due to the shrinkage effect, might potentially be underestimate the true SNR. We also present results of another simulation for  $n \in \{24, 48\}$ ,  $D \in \{190, 380\}$  and  $\text{SNR} \in \{0.01, 0.1, 1\}$  in the appendix. The results suggest that, even for a small number of observations, the estimation performance is satisfactory when the density of sampling is large enough.

The results of our simulation studies are briefly summarised in the following sections. See

the supplementary material for a full presentation of results.

#### 4.1. Estimation of historical effects

Though estimation performance for simple historical effects has already been examined in [Brockhaus et al. \(2016b\)](#), we provide additional simulation results for complex multi-modal effect surfaces. The simulation settings are motivated by our application, in which several time windows may show a relationship between the two biosignals. We thus simulate data sets where the effect surface is multi-modal for both the  $s$ - and the  $t$ -direction. Samples were generated from the model

$$Y_i(t) = \alpha(t) + \int_0^{t-\delta} x_i(s)\beta(s,t)ds + \varepsilon_i(t), \quad i = 1, \dots, n, \quad (16)$$

for which the functional covariate  $x_i(s)$  is simulated as sum of  $\varkappa \in \{5, 7, 9, 11\}$  natural cubic B-Splines with independent random coefficients from a standard normal distribution. The true underlying coefficient surface is given by  $\beta(s, t) = \sin(10 \cdot |s - t|) \cdot \cos(10t)I(s \leq t - \delta)$  with  $I(s \leq t - \delta) = 1$  if  $s \leq t - \delta$ , else 0. The independent Gaussian error process  $\varepsilon(t)$  with mean zero has constant variance  $\sigma^2$  defined via the  $\text{SNR} = \sqrt{\text{Var}(\Xi)}/\sqrt{(\sigma^2)}$  with  $\text{Var}(\Xi)$  being the empirical variance of the linear predictor.

In addition, we simulate effect surfaces with a band structure. This is done by using the data generating process in (16) and restricting the influence of  $x_i$  to values  $s$ , for which  $s \leq t - \delta$ ,  $s \geq t - 0.1$  and  $t \leq 0.75, s, t \in [0, 1]$ . With 40 observed time points the restriction  $s \geq t - 0.1$  corresponds to an autoregressive model with time-varying effects and a lag of  $0.1/(1/40) = 4$  time points. With this simulation, we want to investigate whether our approach is able to adequately recover the effect of  $x_i$  restricted to a certain number of lags without having to predefine lags. This would be an advantage over time-series models which have to specify the assumed lag structure a priori and would allow a corresponding dimension reduction without restricting the analysis.

*Results.* For combinations in which  $n$  and SNR are not very small at the same time, our gradient-boosting approach works well and recovers the true underlying functional relationship. These findings are depicted in Figure 2. As can be seen in the upper row, both `pffr` and `FDboost` are able to recover the true underlying effect well (right panel) with `FDboost` having an advantage for low SNR and low  $n$  (left panel). For higher SNR, where `FDboost` shows less of an improvement than `pffr` compared to the low SNR setting, boosting estimates may potentially be further improved by using a higher number of iterations (limited to 1500 for this subsection). In the supplementary material, we additionally provide estimates with average `reliMSE` for a smaller number of observations, visualising the deterioration in estimation performance with decreasing sample size.

Similar to the multi-modal example, FDboost outperforms pfr (lower row of Figure 2) for band surfaces in settings with a lower SNR, whereas for a SNR = 10, pfr shows partly better performances. As exemplarily shown in the lower right panels of Figure 2, FDboost is often able to correctly detect the non-zero regions, whereas the typical estimated surface of pfr exhibits larger parts with false positive estimates.

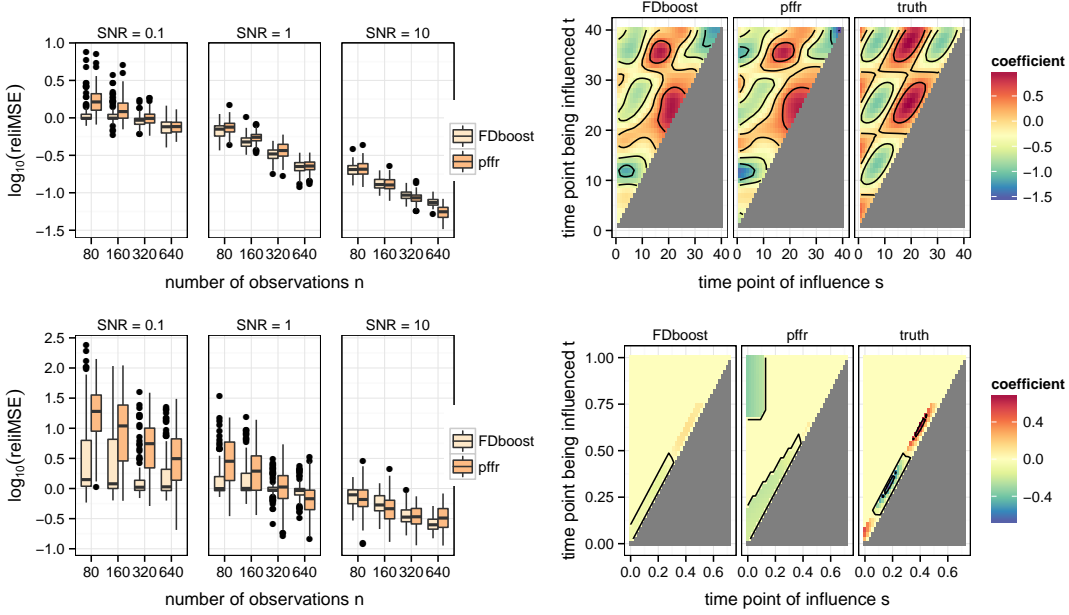


Fig. 2: Left panels: Comparison of reliMSEs for the estimation of multi-modal surfaces (upper row) as well as band surfaces (lower row) and different settings of the SNR (columns). The  $x_i(s)$  were generated on the basis of 11 natural cubic B-Splines with 15 knots. Right panels: example for estimates of a multi-modal surface (upper row) for 640 observed trajectories and a SNR of 1 respectively estimates of a band structured coefficient surface (lower row) for 320 observed trajectories and a SNR of 10 both with respective average reliMSE.

#### 4.2. Estimation performance for factor-specific historical effects

For random historical effects, we adapt the ideas of Scheipl and Greven (2016) and Brockhaus et al. (2016b, Web Appendix C) and generate random coefficient functions  $\beta_f(s, t)$  as linear combinations of cubic P-splines (Eilers and Marx, 1996) for  $n_{\text{subject}} = 10$  factor levels (subjects). The coefficient functions  $\beta_f(s, t)$ ,  $f = 1, \dots, \varphi = 10$  are then centred to comply with constraint (12). For factor-specific historical effects, we specify multiples  $\iota(e)$  of one fixed coefficient function  $\varpi(s, t) = \frac{s}{\sqrt{2}} \cdot \cos(\pi\sqrt{t})$  with  $\iota(e)$  being centred coefficients drawn uniformly between  $-5$  and  $5$  for each factor level  $e = 1, \dots, \eta = 4$ , allowing for a more systematic examination of estimation

accuracy in specific regions of the coefficient function. An additional doubly-varying effect is simulated by multiplying  $\varpi(s, t)$  with centred random coefficients drawn from a standard normal distribution.

In a first series of settings (correctly specified case), the data are generated on the basis of the fitted model, including a main historical effect and (i) a time-varying categorical effect as well as a factor-specific historical effect, (ii) a time-varying random effect as well as a random historical effect, (iii) combining (i) and (ii), or (iv) combining (iii) with a doubly-varying historical effect (full model). In a second series of settings, the model is misspecified by fitting a single historical effect, whereas the data are simulated using a main and (v) a factor-specific historical effect or (vi) a random historical effect or alternatively (vii) by generating the data from the full model whereas the model is fitted without the doubly-varying effect.

*Results.* Whereas the main historical effect for the settings (i)-(iv) shows a similar logarithmic  $\text{reliMSE}$  as in previous simulation settings in 4.1, the historical effects varying with a categorical covariate show more diverse performances and larger deviations. The factor-specific and random historical effect estimation mostly capture the main features of the true underlying surface, but are not estimated as reliably as the main historical effect. Estimates for the doubly-varying historical effect are often shrunk almost to zero due to an insufficient number of observations.

In settings (v) or (vi) where the true underlying model includes a random or factor-specific historical effect, estimation performance for the main historical effect is equally good when fitting the correct or the misspecified model. For setting (vii) the performance is practically the same for the estimation of the main historical effect. The difference in estimation performance varies more strongly for the factor-specific as well as random historical effect and, in particular, indicates a better performance of the correctly specified model for high SNR and larger  $n$ . The fact that estimation performance is not affected more strongly is likely due to the orthogonality of the omitted effect to the effects included in the model, cf. (12) - (14).

### 4.3. Quantification of uncertainty

In the following, we examine the ability of 95%-bootstrap intervals to correctly identify (non-)zero coefficients in the manner of conventional confidence intervals by looking at the inclusion of zero. On the basis of 100 nonparametric bootstrap iterations, we calculate the *false negative rate (FNR)* and *false positive rate (FPR)* over the surface for each of 100 simulated data sets. In addition, the frequencies of false negative (*FFN*) and false positive estimates (*FFP*) for each surface point across all data sets are obtained. We present results for a model including only one main historical effect in addition to a model with main and factor-specific historical effects, for both of which true coefficient surfaces are partly equal to zero. The true coefficient surface for the



main historical effect is defined as  $\beta(s, t) = \mathcal{Q}_{0.001}\{\sin(|t-s|+10)\cdot\cos(5s)\}$  and surfaces for factor-specific historical effects are simulated as multiples of  $\varpi(s, t) = \mathcal{Q}_{0.001}\{\phi_{0.9,0.2}(s) \cdot \phi_{0.9,0.2}(t)\}$ , where  $\mathcal{Q}_a(x) = x \cdot I(x \geq a)$  and  $\phi_{\mu,\sigma}(\cdot)$  is the normal density function with expectation  $\mu$  and variance  $\sigma^2$ . We additionally investigate the performance of our uncertainty quantification for a model including main and random historical effects, which are simulated as described in section 4.2.

*Results.* Figure 3 depicts the results for a simple historical effect simulation with  $\text{SNR} = 1$ ,  $n = 160$  and  $D = 40$ . Both the FNR and the FPR are below 0.05 in all but a few cases. When decreasing the SNR to 0.1, the bootstrap approach yields smaller FPR at the cost of a larger FNR. Considering the FFP and FFN, 8% of all non-zero surface points reveal a FFN of above 0.05 and 30% of all zero surface points reveal a FFP of above 0.05. Plotting the FFN against the coefficient size indicates that FFNs larger than 0.05 only occur for coefficient values of below 0.2 (below 0.6 if  $\text{SNR} = 0.1$ ). The rightmost panel of Figure 3 reveals a strong relationship between the FFP and a smaller distance to non-zero points on the surface, with FFP mostly below about 0.1 for points not next to a non-zero coefficient.

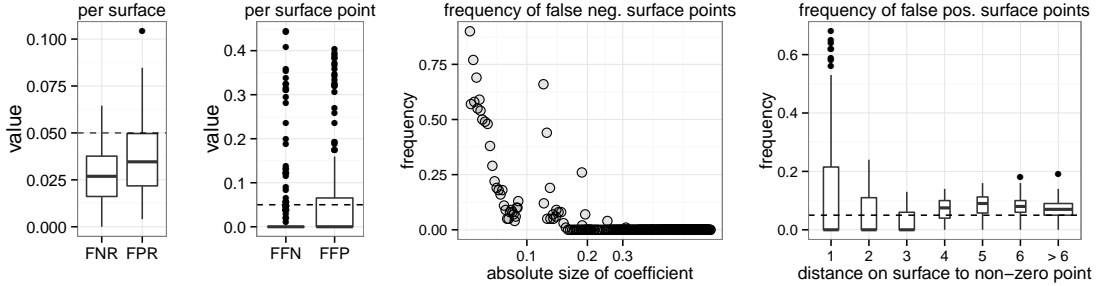


Fig. 3: Results for uncertainty quantification of a simple historical effect and data generated with  $\text{SNR} = 1$ ,  $n = 160$  and  $D = 40$ . FNR and FPR for each surface with boxplot over iterations (left panel) as well as FFN and FFP for each surface point over all simulation iterations with boxplot over surface points (second panel). Third panel: frequency of bootstrap intervals including zero plotted against the coefficient size for each truly non-zero coefficient surface point. Forth panel: frequency of false positive estimates plotted against the minimal distance to a true non-zero point for each zero surface point.

Though the performance depends on the specific surface, the bootstrap approach finds the majority of non-zero coefficient points in simulations for a simple historical model and tends to have a FFN of almost zero. A large FFP only occurs for surface points, that are directly adjacent to true non-zero coefficient points.

For a more complex model also including a factor-specific historical effect, the bootstrap approach works well regarding the detection of the truly non-zero surface area. However, it reveals

considerably higher FNR as well as higher FFN particularly for smaller coefficients of both effect surfaces. In the case of correlated observations, for example given by repeated measurements per subject, we subsample on the level of independent observation units (subjects). In the simulation with a main and a random historical effect, higher frequencies of false positive estimates for the main historical effect occur, which, however, are again located around the true non-zero coefficient area.

In summary, simulation results suggest that the bootstrap approach does not comply with the chosen confidence level in the manner of conventional confidence intervals, but proves to find most of the truly non-zero surface regions for all simulation settings. Large FFN and FFP are mainly revealed at the edges of non-zero coefficient areas, such that an interpretation of detected non-zero areas of the surface are still possible as long as exact pixel locations of edges are not taken at face value.

#### 4.4. *Further simulations*

In addition to the presented simulations, we investigate the performance of boosting for different parameterisations as introduced in section 2.2 and compare boosting estimates with step-length  $\nu = 0.1$  and  $\nu = 1$ . The gradient boosting algorithm is defined for step length  $\nu \in (0, 1]$ . In general, it is recommended to set the step length “sufficiently small” (Bühlmann and Hothorn, 2007) for predictive accuracy reasons, for example in the range of 0.01 and 0.1. A larger step length and, in particular  $\nu = 1$ , requires much fewer iteration steps and therefore speeds up the model fit, but may result in a deterioration of prediction performance due to overfitting. Since we are rather interested in the estimation performance of model components, we investigate whether or how much overfitting is a problem in our particular setting.

*Results.* For the two different parameterisations, performances differ on a relatively small scale, suggesting that the choice of parameterisation can be based on the given research question. In the comparison of step-lengths, there appears to be no clear best choice in all settings. Thus estimation with  $\nu = 1$  might be a reasonable alternative to smaller step-lengths, requiring less computing time and memory consumption due to a smaller number of necessary iterations, especially in complex models applied to large data sets.

## 5. Application to the detection of synchronisation in bioelectrical signals

### 5.1. *Data and background*

Gentsch et al. (2014) conducted a study in which 24 participants played a computerised gambling game with real monetary outcome. During the gambling rounds, Gentsch et al. modi-

fied three factors (so-called appraisals) related to Scherer's Component Process Model (CPM, Scherer, 2009) and simultaneously recorded brain activity with EEG and facial muscle activity with EMG. In componential emotion theories such as the CPM, an emotion episode is assumed to emerge through the synchronisation of the emotion components (e.g., appraisals, expressions, or feelings). In order to investigate synchronisation processes, Gentsch et al. operationalised three dichotomous appraisals, which are included as dummy variables in the present data set: (1) *Goal conduciveness*, which was related to the monetary outcome at the end of each gambling round (*gain* coded as  $G = 1$  or *loss* with  $G = 0$ ), (2) *Power*, which allowed players to change the final outcome if the setting was *high power* (*hp* for short coded as  $P = 1$ , else referred to as *low power / lp* with  $P = 0$ ) and (3) *Control*. The control setting was manipulated in blocks in order to change the participant's subjective feeling about her ability to cope with the situation. Before a block with several gambling rounds would start, participants were told whether they were going to have high or low power for the majority of upcoming games, which corresponds to *high* or *low control* settings (*hc* coded as  $C = 1$  respectively *lc* with  $C = 0$ ). In rounds with high control, for example, the player was told to frequently have high power, thereby trying to induce a subjective feeling of control over the situation, and vice versa for low control. Each participant played over 100 gambling rounds for each of the eight appraisal settings, which we also refer to as *trials*.

Before performing statistical analyses, EEG- as well as EMG-signals are pre-processed (see the supplementary material for further details). After removing the data of one participant due to considerably deviating observations, which imply a defective or displaced sensor, several hundred gambling rounds each with 384 equally spaced EEG- and EMG-measurements within around 1500 milliseconds are available for each of the 23 participants. Analogous to previous studies on synchronisation and, in particular, the study of Gentsch et al. (2014), we use aggregated observations for each participant and game condition by averaging the corresponding trials for each time point. On the one hand, this results in less computing time and the feasibility to quantify uncertainty in effect estimates via bootstrap, on the other hand, this is motivated by investigations on event-related potentials (ERPs). ERP analysis is a commonly practised method to infer from neuronal activity. Neuronal activity is thought to be time-locked in delay to a certain stimulus, wherefore aggregating over a large number of trials is used to cancel out random brain activity and strengthens those parts of the signal, which are commonly observed for all trials (see, e.g., Pfurtscheller and da Silva, 1999; Handy, 2005; Rousselet et al., 2008).

Instead of combining the (spatially correlated) EEG-signals in order to maximize the explanatory power of the analysis, the question of interest rather lies in the dominant influence of certain selected EEG-signals. We fit a model for each EEG-signal of interest ( $Fz$ -,  $FCz$ -,  $POz$ -

and  $P_z$ -electrode) in order to determine the direct effect on the facial muscle activity. In order to demonstrate the capability of our approach to handle high-dimensional data sets, we also provide sample code in the repository for fitting a model, in which all 64 EEG-signals are potentially included with historical, factor-specific and random historical effects. In the supplementary material, we additionally provide a visualisation for the selection frequency of this model after 2000 iterations.

## 5.2. Model

It is predicted that facial expression is largely driven by efferent brain signals reflecting appraisal processes. We use the following maximal model

$$Y_{il}(t) = \sum_{j=1}^{13} h_j(\mathbf{x}_{il})(t) + \varepsilon_{il}(t), \quad (17)$$

for  $l = 1, \dots, n_{\text{setting}} = 8$ ,  $i = 1, \dots, n_{\text{subject}} = 23$ ,  $t \in \mathcal{T} = [0ms, 1500ms]$  and  $D_i \equiv D = 384$  observed time points in  $\mathcal{T}$ . In (17),  $Y_{il}(t)$  represents a chosen EMG-signal for subject  $i$ , game condition  $l$  and time point  $t$  in the game.  $h_j(\mathbf{x}_{il})(t)$ , or, for short,  $h_j(t)$  are thirteen partial effects of covariates  $\mathbf{x}_{il}$  including a time-varying intercept, game condition effects ( $C$ ,  $P$ ,  $G$ ) and EEG-signal effects depending on the selected electrode signal  $\omega_{il}$ . Table 1 provides the details on each part of the linear predictor. For the integration limits, we use  $l(t) = 0$  and a lead-parameter  $u(t) = t - \delta = t - 12ms$ , which is meaningful due to restrictions given by the neuro-anatomy of humans and is just below the time lag between EMG and EEG of  $14.3ms$  (Mima and Hallett, 1999). In order to reflect subject-specific variation, we include time-varying random intercepts and subject-specific historical EEG-effects in the model.

Though game condition-specific historical effects may well be subject specific, simulations in the previous section suggest that even if the true model corresponds to the full model, estimation performance is only slightly affected when using a misspecified model without a random factor-specific historical effect  $h_{13}(t)$ . As a sensitivity analysis, we also fit the full model including  $h_{13}(t)$  on a finer aggregation of the data, for which we average over fewer trials per subject and thus obtain repeated measurements per subject-game condition-combination.

## 5.3. Results

For the historical effects, the estimated coefficient surfaces are depicted in Figure 4 for the EEG-covariate in the form of the electrode 'Fz' (in particular measuring intentional and motivational activities, Teplan (2002)) and the EMG-response signal of the frontalis muscle (raises the eyebrows). The lower panel in these figures depicts the average EEG-signal per game condition,

Table 1: Partial effects in the EMG-EEG-model

| <i>Partial effect</i> $h_j(x_{il})(t)$                         | <i>Effect (of)</i>                                  |
|--|---|
| $h_1(t) = \alpha(t)$   | Intercept   |
| $h_2(t) = b_{0,i}(t)$  | Subject-specific intercepts                         |
| $h_3(t) = \gamma_1(t)C_{il}$                                   | Game condition <i>control</i>                       |
| $h_4(t) = \gamma_2(t)P_{il}$                                   | Game condition <i>power</i>                         |
| $h_5(t) = \gamma_3(t)G_{il}$                                   | Game condition <i>goal conduciveness</i>            |
| $h_6(t) = \gamma_4(t)C_{il}P_{il}$                             | Interaction of <i>control</i> and <i>power</i>      |
| $h_7(t) = \gamma_5(t)C_{il}G_{il}$                             | Interaction of <i>control</i> and <i>goal cond.</i> |
| $h_8(t) = \gamma_6(t)P_{il}G_{il}$                             | Interaction of <i>power</i> and <i>goal cond.</i>   |
| $h_9(t) = \gamma_7(t)C_{il}P_{il}G_{il}$                       | Interaction of all game conditions                  |
| $h_{10}(t) = \int_0^{t-12} \omega_{il}(s)\beta_1(s, t) ds$     | EEG-signal  |
| $h_{11}(t) = \int_0^{t-12} \omega_{il}(s)\beta_{2,l}(s, t) ds$ | EEG-signal (game-condition specific)                |
| $h_{12}(t) = \int_0^{t-12} \omega_{il}(s)b_{1,i}(s, t) ds$     | EEG-signal (subject-specific)                       |
| $h_{13}(t) = \int_0^{t-12} \omega_{il}(s)b_{2,i,l}(s, t) ds$   | EEG-signal (subj.- and game cond.-spec.)            |

demeaned per time point by the overall mean and with negative or positive values highlighted in blue or red, respectively. Two further panels (left, center) for the EMG-signal show the overall mean, the prediction with and without the historical effects (left) as well as the difference between these predictions (center). For predictions, the average EEG-signal per game condition was used. Additionally, corresponding bootstrap results for uncertainty assessment are incorporated in the figures by different degrees of transparency related to different pointwise bootstrap intervals  $BI_\alpha = [q_{\alpha/2}, q_{1-\alpha/2}]$ ,  $q_\alpha$  as  $\alpha\%$ -bootstrap quantile and  $\alpha \in \{1, 5, 10\}$ . Surface points are coloured with the corresponding coefficient value and are less transparent if the specified bootstrap interval does not contain the value zero.

Figure 4 shows the sum of the estimated coefficient surfaces of main and game condition-specific historical effects for the four high control settings (the other four surfaces are included in the online appendix). In all four effect surfaces a similar pattern can be found, which reflects the structure of the main historical effect. The coefficients near the diagonal reveal a positive sign at around  $s \approx 500ms$ , whereas the upper left as well as the upper right of the surface, visually separated by a thick black contour line, are estimated with a negative sign. In contrast to the upper left negative coefficient area, which is mostly indicated to be not different from zero by the bootstrap, the upper right negative coefficient area is indicated to be non-zero for all eight conditions at least to some extent. The positive area in between those two negative subareas is mostly estimated to be either zero or non-zero but with relatively small coefficient values. The positive effect near the diagonal at  $s \approx 500ms$  is estimated to have the largest values for hc settings in combination with hp / loss and lp / gain situations and is found to be non-zero by

the bootstrap only for the latter scenario. This very strong short-term synchronisation of EEG- and EMG-signal seems to be very reasonable from a theoretical point of view, as facial reactions including raising of the eyebrows are usually of brief nature and are linked to appraisals such as novelty, which is consistent in the hc / lp / gain case with low power not being expected in a high control setting (Scherer, 2009).

The estimated effect can on the one hand be interpreted on the subject level. A person with a higher EEG-signal at  $s \approx 500ms$ , for example, will on average show a higher EMG-signal (i.e. stronger muscle activity) for  $t \approx 600ms$ , given the preceding EEG-signal and game condition remain the same. On the other hand, effects can be explained by relating the demeaned average EEG-signal for one game condition and the corresponding coefficients to the changes in the average EMG-signal, which is illustrated by the hc / lp / gain setting in Figure 4. As EEG values related to this game condition are on average above the overall mean EEG values for  $s \in [300, 1000]ms$ , the EEG seems to have an increasing effect on subsequent EMG values and thus muscle activity, with the effect lasting for at least  $100ms$ .

In theory, muscle activity should be traceable to brain signals. Therefore the results indicate that brain activity measured at the  $Fz$ -electrode only contributes to a relatively small amount in explaining the movement of eyebrows (difference panels on the left of each plot in Figure 4). However, for the game condition hc / lp / gain, the model explains a considerable amount of EMG-activity (particularly visible in the difference plot of EMG predictions).

When reparameterising the factor-specific historical effects without historical main effect, when boosting with step-length 1 as well as in the full model with more finely aggregated data, the estimated effects are similar to the reported ones. Further results for the application are given in the online appendix, including results for the scalar covariates.

Gentsch et al. (2014) analysed EEG- and EMG-signals separately and made statements regarding differences in game conditions for one of the signals at a time. Although this and other similar strategies may yield results on significant changes in one signal for different study settings, no statement on the association of the two signals can be made. In contrast, investigating the emotion components data with our proposed approach facilitates the modeling of synchronisation of EMG- and EEG-signals in the first place and additionally allows the simultaneous EEG- and EMG-analysis to differ for influence factors given by the study design. Our method therefore is able to recreate parts of the theoretical emotion components model and leads to new insights on the underlying synchronisation process. Specifically, we found associations between EEG- and EMG-signal that are time-localized (without the need to prespecify time lags) and which differ between experimental settings, with setting hc / lp / gain showing the clearest association.

## 6. Discussion

The focus of this paper is the development of a regression framework for the synchronisation analysis of bioelectrical signal data. Bioelectrical signals like EEG or EMG are recorded in many different research areas, as for example, in neuroscience or cognitive neuropsychology, where the goal is to develop an understanding of synchronisation processes in emotion episodes. In contrast to previous approaches, which are mostly based on coherence, cross-correlation or similar concepts (see, e.g., [Mima and Hallett, 1999](#); [Brown, 2000](#); [Grosse et al., 2002](#)), we use a function-on-function regression model (see, e.g., [Morris, 2015](#)) with factor-specific historical effects. Our model extends the simple historical model ([Malfait and Ramsay, 2003](#); [Harezlak et al., 2007](#); [Brockhaus et al., 2016b](#)) by factor-specific and / or random historical effects. As far as we know, there are no methods available other than `FDboost` allowing historical effects to vary with other covariates. We develop constraints to make the resulting estimates both interpretable as well as identifiable. This flexible class of function-on-function regression models is implemented in the R package `FDboost`. Using the component-wise gradient boosting approach by [Brockhaus et al. \(2015, 2016b\)](#) for estimation, this approach can deal with high-dimensional data, even  $p > n$  settings, and includes variable selection. The algorithm is able to recover different effect surfaces, including relationships assumed in time series approaches, and allows for potentially time-varying associations. The quality of estimates is comparable to those of the function `pffr` of the R package `refund` for special cases of function-on-function regression where `pffr` is applicable.

A bootstrap can be employed to assess the variability of boosted estimates. While bootstrap intervals, due to the shrinkage, do not constitute confidence intervals with proper coverage, simulations show that the bootstrap approach is able to recover areas with non-zero effects very well and only shows a larger FPR and FNR at the edges of true non-zero effect surfaces. A better uncertainty quantification would be a relevant avenue for future developments.

While we do not focus on this feature here, our approach can also model other characteristics of the conditional response distribution than the mean, such as the median or a quantile. A more complex yet interesting class of models would be obtained by combining functional regression models with generalized additive models for location, scale and shape as done for scalar response by [Brockhaus et al. \(2016a\)](#).

For the emotion components data, our model contributes to the understanding of the component theory by estimating a functional relationship between the EEG and EMG signals without having to prespecify a certain time lag between these two signals. In addition, our proposed extension for historical models allows for appraisal-specific investigations on synchronisation processes of emotion components.

## Acknowledgements

We thank Fabian Scheipl for his help and useful comments. Sonja Greven, Sarah Brockhaus and David Rügamer acknowledge funding by Emmy Noether grant GR 3793/1-1 from the German Research Foundation. Kornelia Gentsch and Klaus Scherer were funded by an ERC Advanced Grant in the European Community's 7th Framework Programme under grant agreement No. 230331-PROPEREMO to Klaus Scherer and by the National Center of Competence in Research (NCCR) Affective Sciences financed by the Swiss National Science Foundation (No. 51NF40-104897) hosted by the University of Geneva.

## References

- Binder, H., Porzelius, C. and Schumacher, M. (2009) Rank-based p-values for sparse high-dimensional risk prediction models fitted by componentwise boosting. *Tech. Rep. FDM-Preprint Nr.101*, University of Freiburg, Germany.
- Bortel, R. and Sovka, P. (2006) EEG-EMG coherence enhancement. *Signal Processing*, **86**, 1737–1751.
- Brockhaus, S., Fuest, A., Mayr, A. and Greven, S. (2016a) Signal regression models for location, scale and shape with an application to stock returns. URL: <https://arxiv.org/abs/1605.04281>. Submitted.
- Brockhaus, S., Melcher, M., Leisch, F. and Greven, S. (2016b) Boosting flexible functional regression models with a high number of functional historical effects. *Statistics and Computing*. To appear.
- Brockhaus, S. and Rügamer, D. (2016) *FDboost: Boosting Functional Regression Models*. URL: <http://CRAN.R-project.org/package=FDboost>. R package version 0.2-0.
- Brockhaus, S., Scheipl, F., Hothorn, T. and Greven, S. (2015) The functional linear array model. *Statistical Modelling*, **15**, 279–300.
- Brown, P. (2000) Cortical drives to human muscle: the piper and related rhythms. *Progress in Neurobiology*, **60**, 97 – 108.
- Brumback, B. A., Ruppert, D. and Wand, M. P. (1999) Comment on "Variable selection and function estimation in additive nonparametric regression using a data-based prior". *Journal of the American Statistical Association*, **94**, 794–797.
- Bühlmann, P. and Hothorn, T. (2007) Boosting algorithms: Regularization, prediction and model fitting (with discussion). *Statistical Science*, **22**, 477–505.
- Diab, A., Hassan, M., Boudaoud, S., Marque, C. and Karlsson, B. (2013) Nonlinear estimation of coupling and directionality between signals: Application to uterine EMG propagation. In *2013*



- 35th Annual International Conference of the IEEE Engineering in Medicine and Biology Society (EMBC), 4366–4369. IEEE.
- Eilers, P. H. C. and Marx, B. D. (1996) Flexible smoothing with B-splines and penalties. *Statistical Science*, **11**, 89–121.
- Gentsch, K., Grandjean, D. and Scherer, K. R. (2014) Coherence explored between emotion components: Evidence from event-related potentials and facial electromyography. *Biological Psychology*, **98**, 70 – 81.
- Gervini, D. (2015) Dynamic retrospective regression for functional data. *Technometrics*, **57**, 26–34.
- Grandjean, D. and Scherer, K. (2009) Synchronization (and emotion). In *The Oxford companion to emotion and the affective sciences* (eds. D. Sander and K. Scherer).
- Grosse, P., Cassidy, M. and Brown, P. (2002) EEG-EMG, MEG-EMG and EMG-EMG frequency analysis: physiological principles and clinical applications. *Clinical Neurophysiology*, **113**, 1523 – 1531.
- Handy, T. (2005) *Event-related Potentials: A Methods Handbook*. A Bradford book. MIT Press.
- Harezlak, J., Coull, B. A., Laird, N. M., Magari, S. R. and Christiani, D. C. (2007) Penalized solutions to functional regression problems. *Computational Statistics & Data Analysis*, **51**, 4911–4925.
- Hashimoto, Y., Ushiba, J., Kimura, A., Liu, M. and Tomita, Y. (2010) Correlation between EEG-EMG coherence during isometric contraction and its imaginary execution. *Acta Neurobiol Exp (Wars)*, **70**, 76–85.
- Hofner, B., Hothorn, T., Kneib, T. and Schmid, M. (2011) A framework for unbiased model selection based on boosting. *Journal of Computational and Graphical Statistics*, **20**, 956–971.
- Hollenstein, T. and Crowell, S. (2014) Special issue: Whither concordance? autonomic psychophysiology and the behaviors and cognitions of emotional responsivity. vol. 98, 1–94.
- Hothorn, T., Bühlmann, P., Kneib, T., Schmid, M. and Hofner, B. (2016) *mboost: Model-Based Boosting*. URL: <http://CRAN.R-project.org/package=mboost>. R package version 2.6-0.
- Huang, L., Scheipl, F., Goldsmith, J., Gellar, J., Harezlak, J., McLean, M. W., Swihart, B., Xiao, L., Crainiceanu, C. and Reiss, P. (2015) *refund: Regression with Functional Data*. URL: <http://CRAN.R-project.org/package=refund>. R package version 0.1-13.
- Kang, J. M., Yoo, T. and Kim, H. C. (2006) A wrist-worn integrated health monitoring instrument with a tele-reporting device for telemedicine and telecare. *IEEE Transactions on instrumentation and measurement*, **55**, 1655–1661.
- Kaniasas, E. (2012) *Fundamentals of Biosignals*, 1–26. Springer Berlin Heidelberg.
- Kneib, T. (2013) Beyond mean regression. *Statistical Modelling*, **13**, 275–303.

- Malfait, N. and Ramsay, J. O. (2003) The historical functional linear model. *Canadian Journal of Statistics*, **31**, 115–128.
- Meinshausen, N. and Bühlmann, P. (2010) Stability selection. *Journal of the Royal Statistical Society: Series B (Statistical Methodology)*, **72**, 417–473.
- Mima, T. and Hallett, M. (1999) Electroencephalographic analysis of cortico-muscular coherence: reference effect, volume conduction and generator mechanism. *Clinical Neurophysiology*, **110**, 1892–1899.
- Mima, T., Matsuoka, T. and Hallett, M. (2000a) Functional coupling of human right and left cortical motor areas demonstrated with partial coherence analysis. *Neuroscience Letters*, **287**, 93 – 96.
- Mima, T., Steger, J., Schulman, A. E., Gerloff, C. and Hallett, M. (2000b) Electroencephalographic measurement of motor cortex control of muscle activity in humans. *Clinical Neurophysiology*, **111**, 326 – 337.
- Morris, J. S. (2015) Functional regression. *Annual Review of Statistics and Its Application*, **2**, 321–359.
- Ozaki, T. (2012) *Time Series Modeling of Neuroscience Data*. Chapman & Hall/CRC Interdisciplinary Statistics. CRC Press.
- Pawitan, Y. (2005) Coherence Between Time Series. In *Encyclopedia of Biostatistics*, vol. 2. Wiley Online Library.
- Pfurtscheller, G. and da Silva, F. L. (1999) Event-related EEG/MEG synchronization and desynchronization: basic principles. *Clinical Neurophysiology*, **110**, 1842 – 1857.
- Quiroga, R. Q., Kreuz, T. and Grassberger, P. (2002) Event synchronization: a simple and fast method to measure synchronicity and time delay patterns. *Physical review E*, **66**, 041904.
- Rinn, W. E. (1984) The neuropsychology of facial expression: A review of the neurological and psychological mechanisms for producing facial expressions. *Psychological Bulletin*, **95**, 52.
- Rousselet, G. A., Husk, J. S., Bennett, P. J. and Sekuler, A. B. (2008) Time course and robustness of erp object and face differences. *Journal of Vision*, **8**, 3.
- Ruppert, D., Wand, M. P. and Carroll, R. J. (2003) *Semiparametric regression*. Cambridge series in statistical and probabilistic mathematics. Cambridge and New York: Cambridge University Press.
- Scheipl, F. and Greven, S. (2016) Identifiability in penalized function-on-function regression models. *Electronic Journal of Statistics*, **10**, 495–526.
- Scheipl, F., Staicu, A.-M. and Greven, S. (2015) Functional additive mixed models. *Journal of Computational and Graphical Statistics*, **24**, 477–501.

- Scherer, K. R. (2009) The dynamic architecture of emotion: Evidence for the component process model. *Cognition and Emotion*, **23**, 1307–1351.
- Semmlow, J. L. and Griffel, B. (2014) *Biosignal and medical image processing*. CRC press.
- Teplan, M. (2002) Fundamentals of EEG measurement. *Measurement Science Review*, **2**, 1–11.
- Wood, S. N. (2006) *Generalized Additive Models: An introduction with R*. Chapman & Hal/CRC, Boca Raton, Florida.
- Zhang, T. and Yu, B. (2005) Boosting with early stopping: Convergence and consistency. *The Annals of Statistics*, **33**, 1538–1579.

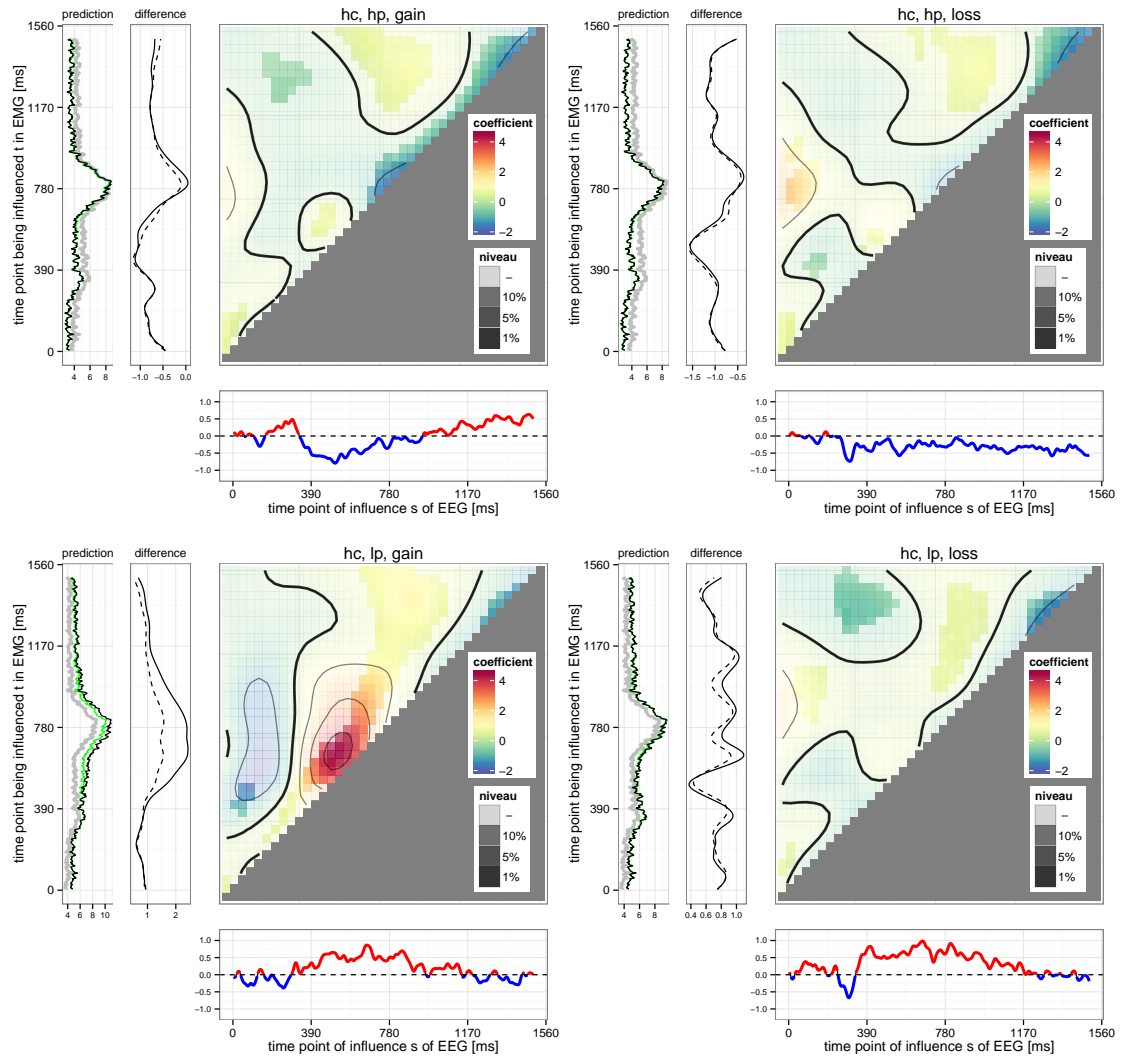


Fig. 4: Estimated coefficient surfaces for the model with EEG-covariate 'Fz' (plot of average signals per game condition at bottom with negative and positive values highlighted blue and red, respectively; signals are demeaned per time point by the overall mean), all four high control settings and the EMG-response signal of the frontalis-muscle (left panels: overall mean (1) in grey, prediction without historical effects (2) in green, with historical effects (3) using the average EEG-signal per game condition in black; center panel: dashed line as difference between (1) and (2), solid line as difference between (1) and (3)). Surfaces correspond to estimated main historical effect plus game condition specific historical effect. Different degrees of transparency in coefficient plot indicate surface points having  $(1 - \text{niveau})$ -bootstrap intervals which do not contain the value zero. To obtain a reasonably sized image estimated effects are visualised on a  $40 \times 40$  grid